DØ Note 5977-CONF

Search for the standard model Higgs boson in the $WH \to \tau\nu b\bar{b}$ channel in 4.0 fb^{-1} of $p\bar{p}$ collisions at $\sqrt{s} = 1.96$ TeV

The DØ Collaboration
URL: http://www-d0.fnal.gov/
(Dated: November 16, 2009)

A search for the standard model (SM) Higgs boson is performed using 4.0 fb^{-1} of $p\bar{p}$ collision data at $\sqrt{s} = 1.96$ TeV, collected with the D0 detector at the Fermilab Tevatron. The final state considered is a pair of b jets, large missing transverse energy and one hadronic τ decay as expected from the reaction $p\bar{p} \to WH \to \tau\nu b\bar{b}$. Boosted decision trees are used to discriminate signal from SM background. Good agreement is observed between data and expected backgrounds, and, for a Higgs boson mass of 115 GeV, a lower limit is set at 95% C.L. on the Higgs production cross section multiplied by the branching fraction for $(p\bar{p} \to (Z/W) + H) \times (H \to b\bar{b})$, which is $14\sigma_{SM}$.

Preliminary Results for the HCP 2009 Conference

I. INTRODUCTION

The search for $p\bar{p} \to WH$, with $H \to b\bar{b}$ and $W \to \tau\nu$, contributes to the overall sensitivity in the search for a low mass standard model Higgs search at the Tevatron, complementing searches in the $W \to (e, \mu)\nu$ final states [1]. The D0 collaboration recently published a first search for this process in hadronic τ decays, based on 1.0 fb^{-1} of integrated luminosity [2]. This note presents an extension of this search to 4.0 fb^{-1}, superseding the 1.0 fb^{-1} result for this channel. The search also includes ZH signal events where one of the τ leptons from the Z decay is not identified. A lower mass limit of 114.4 GeV was set by the LEP experiments for the Higgs boson from analyses of the reaction $e^+e^- \to ZH$ [3], while an upper limit of 157 GeV can be inferred from precision electroweak data [4]. All limits quoted in this Note are at the 95% confidence level.

The final state topology considered in this analysis is a pair of b jets from the decay of the Higgs boson, with missing transverse energy ($\not\!\!E_T$) and a hadronically decaying τ lepton (τ_h). The main backgrounds arise from $(W/Z)b\bar{b}$, from (W/Z)+(non-b jets) due to flavor misidentification (mistagging), from top quark production, from diboson production, and from multijet events with fake $\not\!\!E_T$ resulting from fluctuations in jet energy measurements and with real b jets or mistagged light parton jets.

A series of kinematic selections is first applied to reject most of the multijet events. Jets expected to arise from Higgs boson decays are next required to be tagged as b jets, using a neural network b-tagging algorithm. Finally, discrimination between the signal and the remaining backgrounds is achieved by a boosted decision tree technique.

II. DATA AND SIMULATIONS

The D0 detector [5] consists of a silicon microstrip vertex detector and a fiber tracker, both located within a 2 T superconducting solenoidal magnet. A liquid-argon and uranium sampling calorimeter, housed in three cryostats, provides pseudorapidity coverage out to $|\eta| = 4.2$ with pseudo projective towers of size 0.1×0.1 in (η, ϕ), where η is the pseudorapidity with respect to the proton beam direction and ϕ is the azimuthal angle. It is segmented longitudinally into four electromagnetic (EM) and up to five hadronic layers. Additional shower sampling is provided by scintillating tiles located at the boundaries between cryostats. Beyond the calorimeter, a muon detector consists of tracking detectors and scintillation trigger counters before and after 1.8 T iron toroids.

Online event selection is accomplished with a three-level trigger system. For this analysis, the data were recorded using a set of triggers designed to select events with jets and missing transverse energy. At the highest trigger level, the main requirement through winter 2006 (Run IIa) was $\not\!\!H_T > 30$ GeV, where $\not\!\!H_T = |-\Sigma \overrightarrow{p}_{T\mathrm{jet}}|$ is a measure of missing transverse energy based on jets only. For data collected since spring 2006 (Run IIb), the trigger system was improved [6], allowing in particular the $\not\!\!E_T$ to be used at the first level, and the $\not\!\!H_T$ threshold to be lowered to 25 GeV. Other changes occurred between Run IIa and Run IIb: an additional layer for the silicon tracker was installed close to the beam pipe, thus improving charged particle momentum resolution and heavy flavor identification; the quality and the stability of the calibration of the scintillating tiles of the inter-cryostat detector were also greatly improved.

After data quality requirements, the total integrated luminosity [7] available for this analysis was (4.0 ± 0.2) fb^{-1}. This analysis used charged particle tracks, the primary interaction vertex, calorimeter jets reconstructed in a cone of radius 0.5 by the iterative midpoint cone algorithm [8] with $p_T > 15$ GeV and τ leptons identified using a neural network algorithm [9]. The $\not\!\!E_T$ was reconstructed as the opposite of the vectorial sum of the transverse energies of all energy deposits in the calorimeter. Unless otherwise specified, $\not\!\!E_T$ was corrected for reconstructed muons. The jet energy calibration was performed by requiring transverse energy balance in photon+jet events, and this calibration was propagated to $\not\!\!E_T$.

Except for the background from multijet production, which was estimated from the data, all backgrounds from standard model (SM) processes were determined by Monte Carlo simulation. The (W/Z)+jets processes were generated with ALPGEN [10] interfaced with PYTHIA [11] for initial and final state radiation, and for jet hadronization. A matching algorithm [12] was applied to avoid double counting in phase space regions which can be populated both by ALPGEN or by PYTHIA. Light (u, d, s, g) and heavy (c, b) flavor production in association with W/Z were generated separately, and care was taken to avoid double counting between heavy flavor jets produced directly by ALPGEN or subsequently by PYTHIA. Events were reweighted so that the resulting Z p_T spectrum matches the D0 measurement [13]. The W p_T spectrum was reweighted as well, based on the same input but taking into account the differences between the Z and W spectra predicted by a NNLO computation [14]. For $t\bar{t}$ and electroweak single top production, the ALPGEN and COMPHEP [15] generators interfaced with PYTHIA were used, respectively, while the vector-boson pair production processes were generated with PYTHIA. The signal processes (ZH and WH) were generated with PYTHIA for Higgs boson masses ranging from 100 to 150 GeV, in 5 GeV steps. In all these simulations, the CTEQ6L1 parton distribution functions (PDFs) were used [16].

For the (W/Z)+jets processes, the absolute normalizations were obtained from a next-to-next-to leading order (NNLO) calculation of the total cross sections. The heavy flavor fractions were obtained using MCFM [17]. The cross sections for the other background processes were taken from Refs. [18], or calculated with MCFM, and the signal production cross sections were taken from Ref. [19].

Signal and background samples are passed through full GEANT3-based simulations [20] of the detector geometry and response, and processed with the same reconstruction program as used for data. Datea events from randomly selected beam crossings are overlaid on simulated events to account for additional minimum-bias interactions. Trigger conditions on jets and $\not\!\!E_T$ are not included in the simulation, but parameterizations of trigger efficiency are applied, as determined in data from triggers based only on information from the muon detectors, and therefore independent of those used in this analysis. Weight factors are also applied to compensate for residual differences between data and simulation of luminosity profile, the longitudinal distribution of primary vertices, electron, muon and jet identification efficiencies. The jet energy calibration and resolution are adjusted in simulated events to match those measured in data.

III. EVENT SELECTION

The goal of the preselection criteria is to eliminate the bulk of the otherwise overwhelming background from multijet events, while retaining a high efficiency for the signal. In a second stage, further enhancement of the search sensitivity is achieved using b tagging. The analysis is optimized for a Higgs boson mass of 115 GeV.

The event primary vertex has to be reconstructed within the acceptance of the silicon vertex detector ($|z_{\rm PV}| < 40$ cm, where z is measured from the detector center along the beam direction), and at least three charged particle tracks have to originate from that vertex. Jets associated with charged particle tracks meeting minimal quality criteria such that the b-tagging algorithm can operate efficiently are denoted "taggable" in the following. There have to be at least two taggable jets. These jets must have $p_T > 20$ GeV and $|\eta| < 2.5$ and they must be separated from the tau candidate by $\Delta R(\tau, jet) > 0.5$. Finally, a minimum missing transverse energy is required, $\not\!\!E_T > 15$ GeV.

A tau candidate passing specific cuts for each tau type is required in each event. No requirements are made on other tau candidates in the event, however it is found that there are very few events which contain more than one tau candidate. Two types of one-prong τ decays are considered:

Type-1: Calorimeter cluster, with one associated track and no EM subcluster. This corresponds mainly to the decay $\tau^{\pm} \to \pi^{\pm}\nu$.

Type-2: Calorimeter cluster, with one associated track and at least one EM subcluster. This corresponds mainly to the decay $\tau^{\pm} \to \pi^{\pm}\pi^0\nu$.

The hadronic tau neural network output (τ_{nn_h}) uses a number of isolation and tracking criteria to discriminate taus from jet fakes. Further selections are applied on the τ transverse momentum measured by the calorimeter, p_T, and by the tracks associated to the tau, $p_{T_{trk}}$, and the pseudorapidity of the τ measured with respect to the center of the detector, η_d. The selection criteria for tau candidates are

- Type-1 Taus:
  $p_T > 12$ GeV
  $p_{T_{trk}} > 7$ GeV
- Type-2 Taus:
  $p_T > 10$ GeV
  $p_{T_{trk}} > 5$ GeV

and $|\eta_d| < 2.0$. Initially, $\tau_{nn_h} > 0.3$ is required to suppress jets faking taus which is then raised to 0.9 for the final tau selection. The efficiency for a hadronic tau in this kinematic range to pass the $\tau_{nn_h} > 0.9$ requirement is about 65%. Any events selected in the low mass Higgs searches $WH \to (e, \mu)\nu b\bar{b}$ [1] and $ZH \to \tau\tau jj$ [21] are also rejected to avoid event overlap between the search channels.

After preselection, further criteria are imposed to yield four distinct samples:

- An analysis sample in which the search for a Higgs boson signal is performed;
- a multijet enriched sample to estimate the multijet background;

TABLE I: Numbers of signal and background events expected and numbers of events observed before b tagging, with a single b tag, and with a double b tag. The numbers for the signals are given for a Higgs boson mass of 115 GeV; "top" includes pair and single top production; VV stands for the sum of all diboson processes. The errors quoted are statistical only.

Sample	signal	W+jets	Z+jets	top	VV	multijet	Total	Observed
Pretag	2.1 ± 0.1	6335 ± 22	173 ± 4	278 ± 1	200 ± 1	669 ± 12	7686 ± 26	7512
1-tag	0.80 ± 0.06	181 ± 1	16.0 ± 0.4	100.2 ± 0.4	10.1 ± 0.1	53 ± 3	341 ± 4	343
2-tags	0.94 ± 0.07	66.3 ± 0.4	6.6 ± 0.3	73.7 ± 0.3	4.5 ± 0.1	20 ± 2	171 ± 3	159

- a multijet control sample which is used to validate the multijet modeling, and
- a further control sample for all non-multijet, simulated SM background in which the multijet contamination is expected to be minimal.

The multijet enriched sample is selected by requiring the τ neural network output to lie in the range $0.3 < \tau_{nn_h} < 0.7$. All simulated SM backgrounds that fall into this region are subtracted. This sample is used to estimate the multijet contribution. The multijet control sample is defined such that the contribution from non-multijet processes is minimal. In this definition the $\not\!\!E_T$ significance $\mathcal{S}$ is used which takes into account the resolution of jet energies to assess the significance of the observed $\not\!\!E_T$ relative to expected fluctuations in measured jet energies. Large $\mathcal{S}$ means that it is more likely that the observed $\not\!\!E_T$ is not due to such fluctuations. The requirement $\mathcal{S} < 3.5$ and azimuthal angle $\Delta\phi(\not\!\!p_T, \not\!\!E_T) > 2$ selects poorly reconstructed multijet events in which a jet misidentified as a tau is nearly collinear with $\not\!\!E_T$. To improve the modeling of the multijet background, events in the multijet enriched sample are reweigthed so that the resulting p_T and η distributions of the tau candidates match the distributions in the multijet control sample.

Finally, the control sample with a small multijet contamination is defined by requiring $\not\!\!E_T > 80$ GeV and $\tau_{nn_h} > 0.9$. In general, good agreement is observed between the background expectation and the data in the control samples.

Several kinematic variables, the dijet invariant mass, the $\not\!\!E_T$ significance $\mathcal{S}$ and the τ transverse momentum, are shown in Figure 1 for the preselected data sample compared to the sum of the multijet background and the simulated SM backgrounds. To select the final analysis sample, the threshold on tau neural network is increased to $\tau_{nn_h} > 0.9$, $\mathcal{S}$ is required to be greater than 4.5, and the azimuthal angle $\Delta\phi(\not\!\!p_T, \not\!\!E_T) < 2$.

In Figure 2 the dijet mass and the tau transverse momentum are shown before b tagging for the final signal selection. The combination of multijet events and simulated SM backgrounds provides a good description of the data.

The large branching fraction for $H \to b\bar{b}$ is exploited by requiring that at least one of the two leading taggable jets be b tagged, using cuts on the outputs of the b-tagging algorithm neural network [22]. These cuts were chosen such that either both jets are tagged with a high efficiency but lower purity ("loose tag"), or that one of the two jets was tagged with a lower efficiency but higher purity ("very tight tag"). In order to account for differences in track reconstruction efficiencies in data and in simulation, flavor-dependent scale factors measured in dedicated data samples are applied to the b-tagging efficiencies in the simulation. The effect of b tagging can be observed in Fig. 3, where the simulation also provides a good description of the analysis sample in the single and double b-tag samples, respectively. Details of the signal and background expected numbers of events are given in Table I, as well as the numbers of selected events.

IV. DISCRIMINANT

A boosted decision tree technique [23] is used to take advantage of different kinematic characteristics in signal and background processes. Boosting is a technique whereby a decision tree (DT) is retrained, with a larger weight given to events misclassified in the previous iteration. For each of the probed M_H, the DT trainings is performed on one third of the signal and background samples, for twenty boosting cycles. The remaining two thirds is used to extract the results.

The DTs are trained after b tagging so as to discriminate the signal from all background, except the contribution from multijets. A total of 15 kinematic input variables are presented to the DT. The variable with greatest discriminating power is the dijet invariant mass, m_{jj}. Other variables are:

- p_T and η of the two leading jets
- missing transverse energy $\not\!\!E_T$
- the azimuthal angle between the two jets

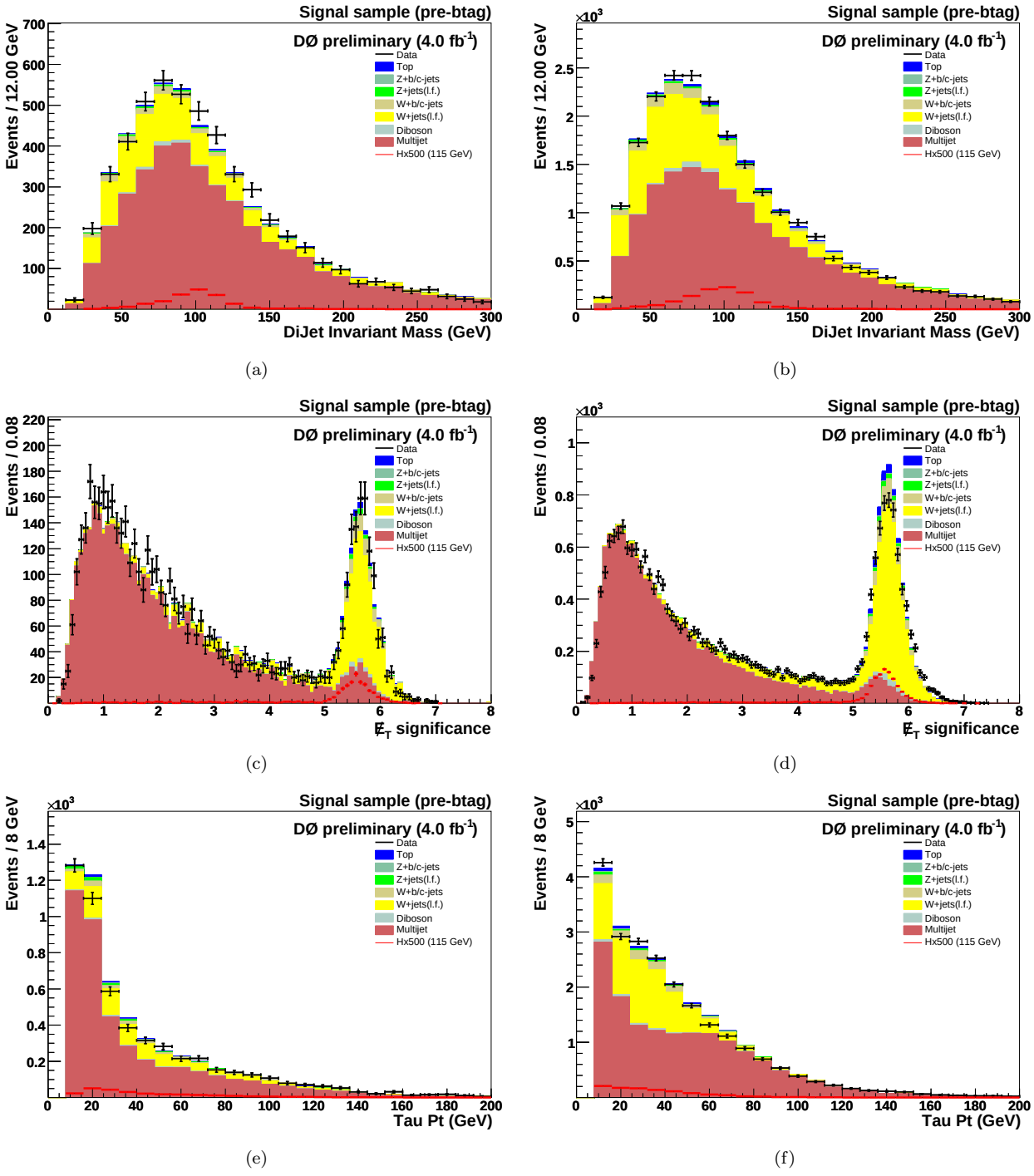

FIG. 1: Distributions in the preselection sample for Type-1 (left column) and Type-2 (right column) events, for (a,b) dijet mass, (c,d) $\not\!\!E_T$ significance and (e,f) transverse momentum of τ_h. The data are shown as points with error bars. The SM background contributions are shown as histograms, with color codes defined in the legends.

- the azimuthal angle between the tau and $\not\!\!E_T$
- the transverse mass of the W boson, m_T
- the tranverse momentum of the τ_h
- the transverse momentum of the charged particle track of the τ_h.

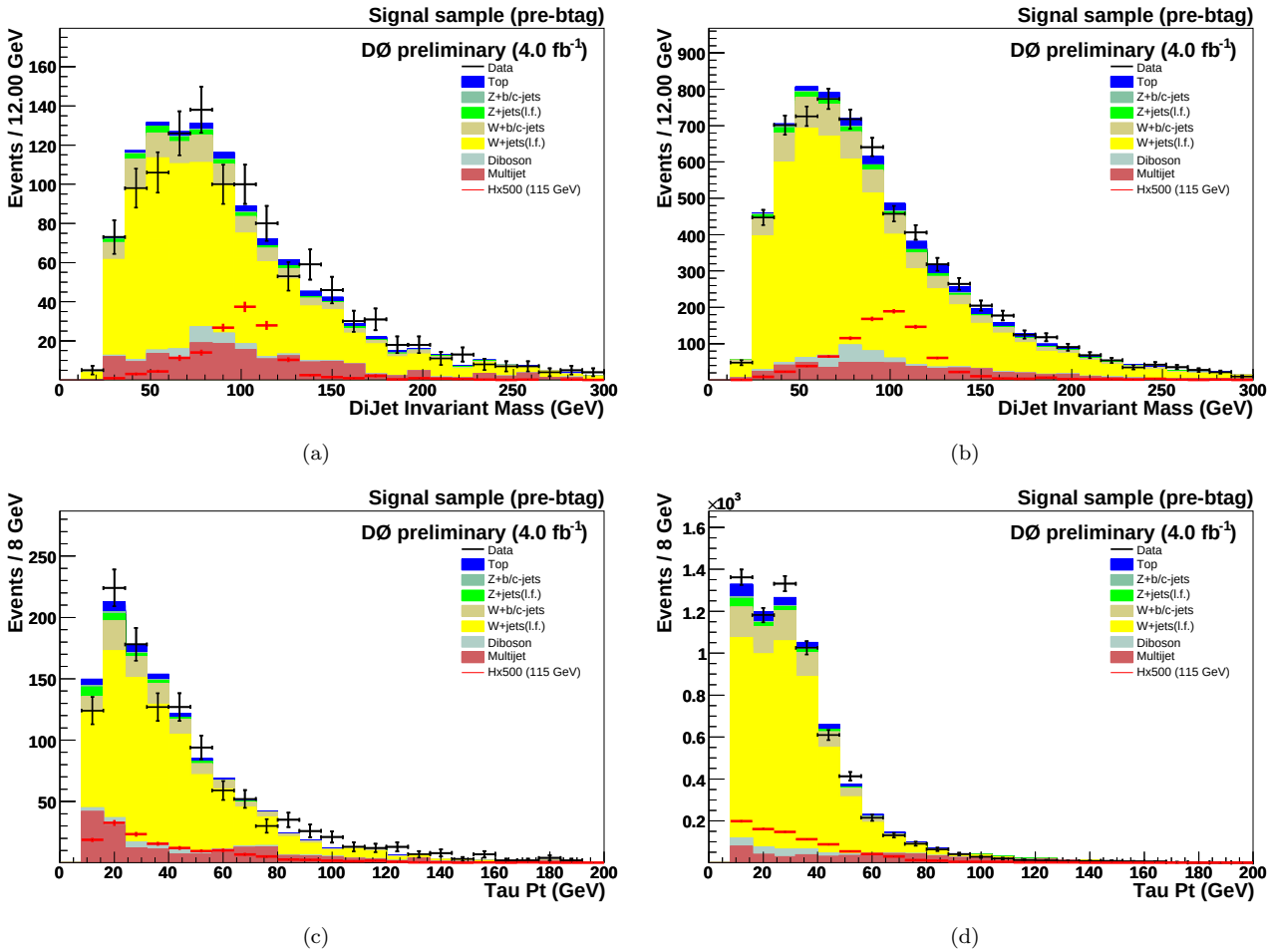

FIG. 2: Distributions in the final signal sample, but before b tagging, for Type-1 (left column) and Type-2 (right column) events: (a,b) for dijet mass and (c,d) transverse momentum of τ_h. The data are shown as points with error bars. The SM background contributions are shown as histograms, with color codes defined in the legends. The distributions for signal are multiplied by a factor of 500.

- H_T and $\not\!\!H_T$
- the asymmetry $(H_T - \not\!\!H_T)/(H_T + \not\!\!H_T)$

The variables H_T and $\not\!\!H_T$ now include the τ_h. i.e., H_T is the scalar sum of the transverse momenta of all jets and taus and $\not\!\!H_T$ is the negative of the transverse component of the net momentum of all jets and τ_h. The DT is trained for Type-1 and Type-2 τ_h, for a total of two and three jets, and one and two b-tags, yielding eight independent channels. The DT output is shown in Fig. 4 for $M_H = 115$ GeV for two Type-1 and Type-2 τ_h, with only two jets which are also b-tagged.

V. SYSTEMATIC UNCERTAINTIES

Systematic uncertainties originate from many sources including trigger simulation, τ_h identification, jet energy calibration, resolution, reconstruction efficiency, and b tagging. The corresponding parameterizations applied in the simulations are varied within their uncertainties, and the impact on the normalizations and the shapes of the DT discriminants are assessed. Correlations among systematic uncertainties for signal and background processes are taken into account in obtaining the final results, as is the uncertainty on the integrated luminosity of the data sample.

Cross sections for the SM processes also have theoretical uncertainties. For the (W/Z)+jets process, the uncertainty on the overall normalization is taken as 6%. Uncertainties on heavy-flavor fractions can be estimated with MCFM, and are set to 20% to encompass additional effects, such as ambiguities in masses of heavy quarks. For other background

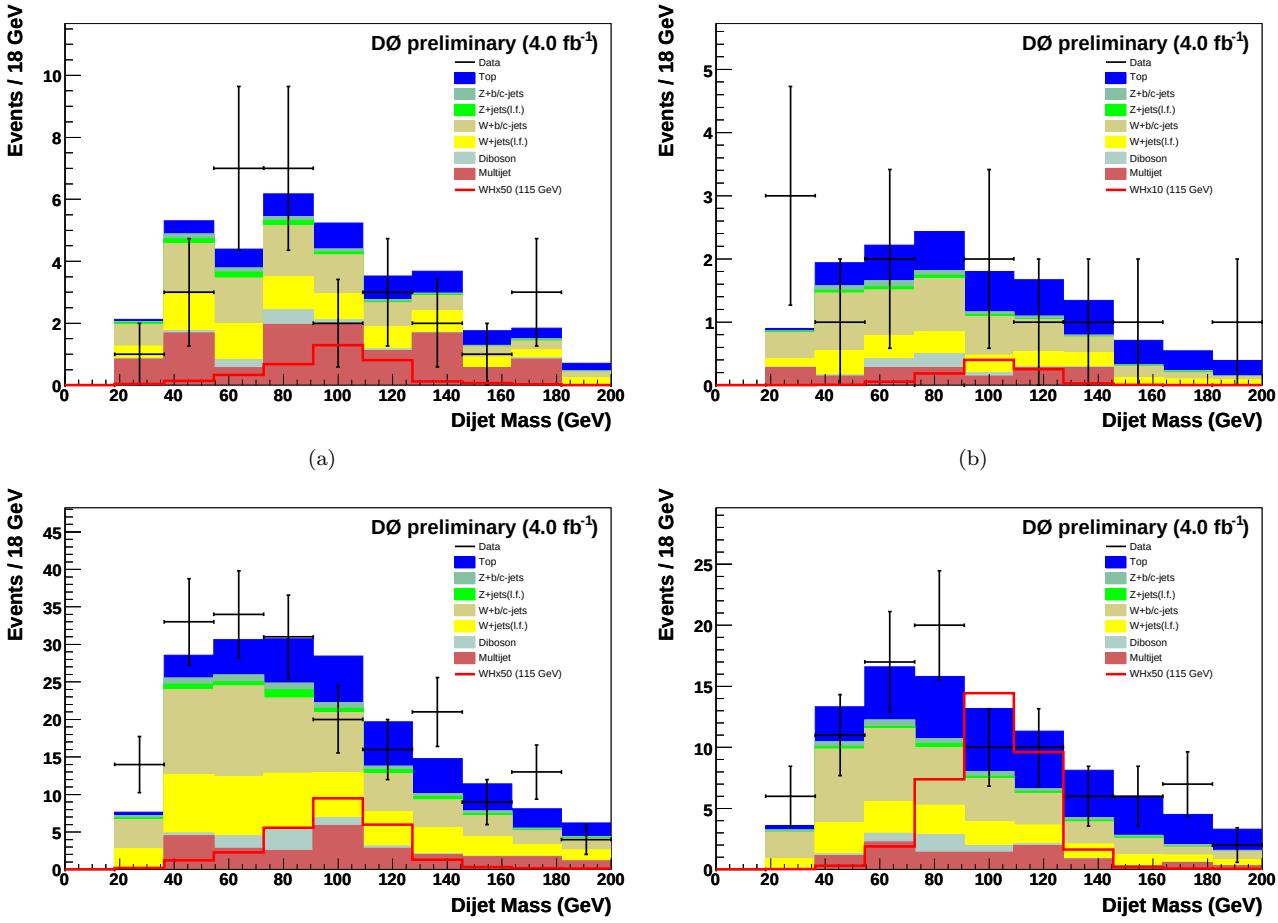

FIG. 3: Dijet mass distributions in the final sample, after b tagging, for Type-1 (top row) and Type-2 (bottom row) events: (a,c) one b-tag and (b,d) two b-tags. The data are shown as points with error bars. The SM background contributions are shown as histograms, with color codes defined in the legends. The distributions for signal are multiplied by a factor of 50.

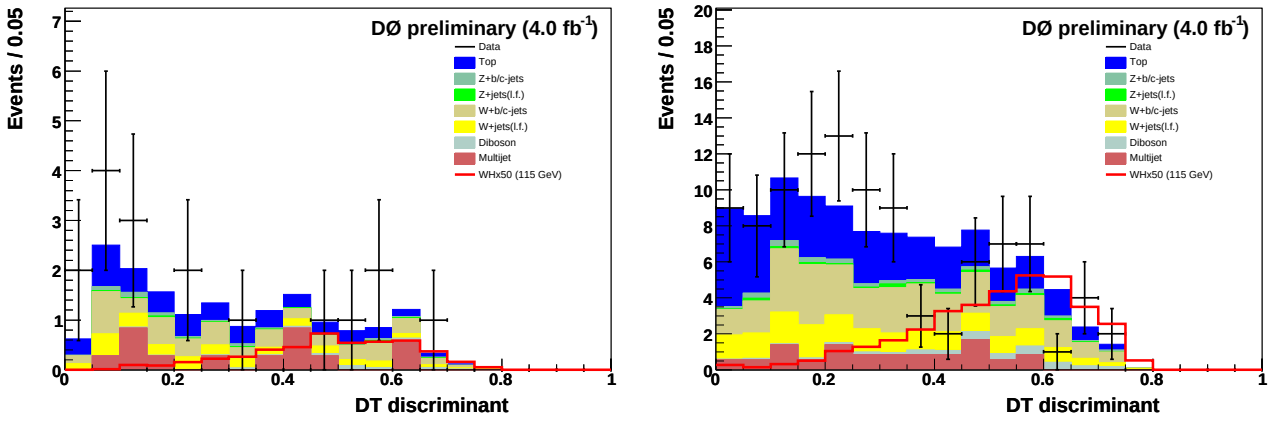

FIG. 4: Decision tree outputs for $M_H = 115$ GeV for (a) Type-1 and (b) Type-2 τ_h decays in events with two jets, with both b tagged. The data are shown as points with error bars. The background contributions (SM and multijet) are shown as histograms, with color codes as indicated in the legends. The distributions signal are multiplied by a factor of 50.

processes, theoretical uncertainties are taken from Refs. [18], or calculated with MCFM. These range from 6% to 10%. The uncertainty on the multijet background is estimated by considering the excursions in integrated number of events after all selections, before and after applying the τ_h reweighting in p_T and η and when the reweighting is not applied. The uncertainty is found to be 12% for Type-1 and 7% for Type-2 events. The uncertainties on the cross sections for signal (6% for $m_H = 115$ GeV) are taken from Ref. [19]. The uncertainties on signal acceptance from the choice of PDF are estimated using the CTEQ6.1M PDF error sets [16], and propagated to the DT discriminants.

VI. RESULTS

Agreement is observed between data and expectation from SM and multijet backgrounds, both in terms of numbers of selected events (Table I) and final distributions in DT discriminants (Fig. 4). To set limits on the $W/Z+H$ production cross section, a modified frequentist approach [24] is used for establishing confidence level CL_s, by defining the ratio of confidence levels for signal+background to the background-only hypothesis ($CL_s = CL_{s+b}/CL_b$), through an integration of the distributions of a test statistic over outcomes of pseudo-experiments, generated according to Poisson statistics, for signal+background and background-only. The test statistic is calculated as a joint log-likelihood ratio (LLR) by summing LLR values over the bins in the DT discriminants. Systematic uncertainties are incorporated via Gaussian smearing of the Poisson probability distributions for signal and backgrounds within the pseudo-experiments. All correlations between signal and backgrounds were maintained. To reduce the impact of systematic uncertainties on the sensitivity of the analysis, the individual signal and background contributions were fitted to the data (and pseudo-data) for both the signal-plus-background and the background-only hypotheses independently by maximizing a profile likelihood function for each hypothesis [25]. The profile likelihood is constructed via a joint Poisson probability over the number of bins in the calculation and is a function of the nuisance parameters in the system and their uncertainties, which are given an additional Gaussian constraint associated with their prior predictions. The maximization of the likelihood function is performed over the nuisance parameters.

The results obtained are shown as a function of M_H in Fig. 5 and in Table II in terms of ratios of excluded to SM production cross sections multiplied by the branching fraction for $H \to b\bar{b}$. The LLRs are also shown in Fig. 5. The observed limit is in agreement with the expected limit, defined as the median of the limits obtained in background-only pseudo experiments. For a $M_H = 115$ GeV, the observed and expected limits on the combined ZH and WH production cross section multiplied by the branching fraction for $H \to b\bar{b}$ are, respectively, a factor of 14.1 and 22.4 larger than the SM value.

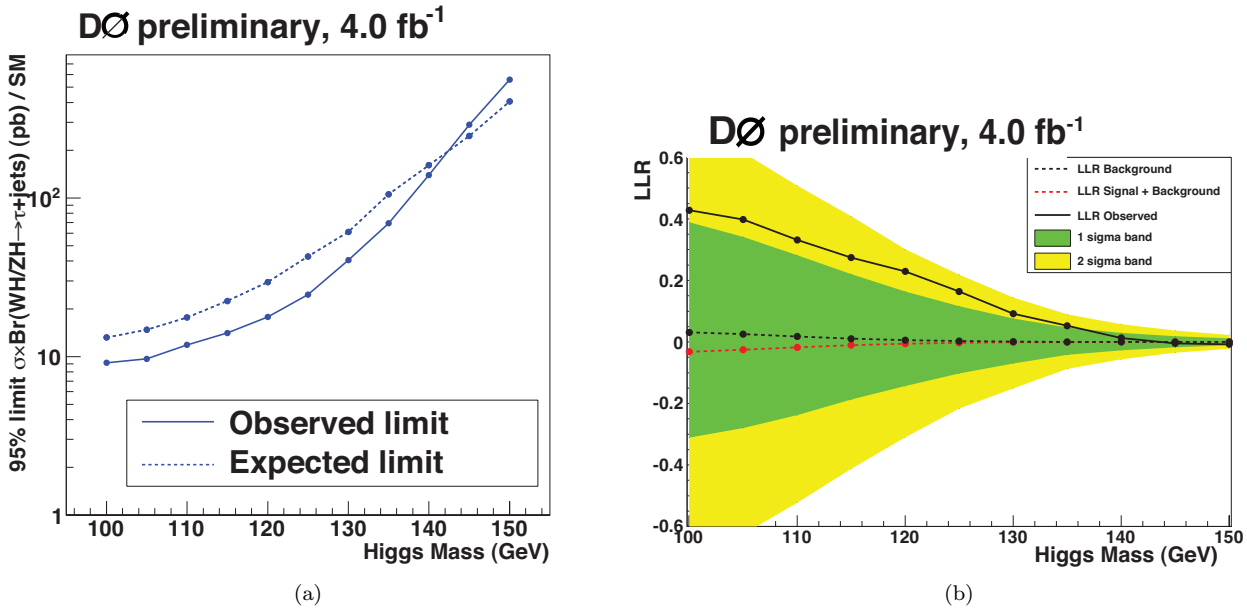

(a) (b)

FIG. 5: (a) Limit on the combined ZH and WH production cross section multiplied by the branching fraction for $H \to b\bar{b}$ as a function of M_H, relative to the SM value, and (b) log likelihood ratio as a function of M_H. In (a) the observed and expected limits are shown as solid and dashed curves, respectively. In (b) the observed LLR is shown as a solid curve, the expected LLRs as black and red dashed curves for the background-only and signal+background hypotheses, respectively, and the green and yellow areas correspond to one and two standard deviations around the expected background-only LLR.

TABLE II: The observed and expected ratio of the values of excluded to SM production cross sections multiplied by the branching fraction for $H \to b\bar{b}$, as a function of M_H.

M_H (GeV)	100	105	110	115	120	125	130	135	140	145	150
observed	9.1	9.7	11.9	14.1	17.8	24.6	40.6	69.1	140	290	557
expected	13.2	14.8	17.7	22.4	29.6	42.8	61.2	105	161	247	406

VII. SUMMARY

A search has been performed for the standard model Higgs boson in 4.0 fb^{-1} of $p\bar{p}$ collisions at $\sqrt{s} = 1.96$ TeV. The topology consists of a pair of b jets, missing transverse energy $\not\!\!E_T$, and a hadronic tau decay, as expected from $p\bar{p} \to WH \to \tau\nu b\bar{b}$ decays. The search is also sensitive to ZH production, where the Z decays into two τ leptons and one is not detected. No deviation is observed from expected SM backgrounds. A boosted decision tree technique is used to derive an upper limit on the combined cross section for $p\bar{p} \to WH$ and $p\bar{p} \to ZH$, as a function of the Higgs boson mass, which for a mass of 115 GeV yields a limit that is factor 14 larger than the expectation from the SM.

Acknowledgments

We thank the staffs at Fermilab and collaborating institutions, and acknowledge support from the DOE and NSF (USA); CEA and CNRS/IN2P3 (France); FASI, Rosatom and RFBR (Russia); CNPq, FAPERJ, FAPESP and FUNDUNESP (Brazil); DAE and DST (India); Colciencias (Colombia); CONACyT (Mexico); KRF and KOSEF (Korea); CONICET and UBACyT (Argentina); FOM (The Netherlands); STFC and the Royal Society (United Kingdom); MSMT and GACR (Czech Republic); CRC Program, CFI, NSERC and WestGrid Project (Canada); BMBF and DFG (Germany); SFI (Ireland); The Swedish Research Council (Sweden); CAS and CNSF (China); and the Alexander von Humboldt Foundation (Germany).

[1] D0 Collaboration, *"Search for WH associated production using neural networks with 5.0 fb^{-1} of Tevatron data"* , D0 Note 5972-CONF (2009).
[2] V.M. Abazov *et al.* (D0 Collaboration), Phys. Rev. Lett. **102**, 251801 (2008).
[3] R. Barate *et al.* [LEP Working Group for Higgs boson searches], Phys. Lett. B **565**, 61 (2003).
[4] The LEP Electroweak Working Group, *"Status of August 2009"*, `http://lepewwg.web.cern.ch/LEPEWWG/`.
[5] V.M. Abazov *et al.* (D0 Collaboration), Nucl. Instrum. Methods in Phys. Res. A **565**, 463 (2006).
[6] M. Abolins *et al.*, Nucl. Instrum. Methods in Phys. Res. A **584/1**, 75 (2007).
[7] T. Andeen *et al.*, *"The D0 experiment's integrated luminosity for Tevatron Run IIa"*, FERMILAB-TM-2365 (2007).
[8] G.C. Blazey *et al.*, in *Proceedings of the Workhop: "QCD and Weak Boson Physics in Run II"*, edited by U. Baur, R.K. Ellis, and D. Zeppenfeld (Fermilab, Batavia, IL, 2000), p. 47; see Sec. 3.5 for details.
[9] V.M. Abazov *et al.* (D0 Collaboration), Phys. Rev. **D** 71, 072004 (2005);
V.M. Abazov *et al.* (D0 Collaboration), Phys. Lett **B** 670, 292 (2009).
[10] M.L. Mangano *et al.*, JHEP **0307**, 001 (2003); version 2.11 was used.
[11] T. Sjöstrand, S. Mrenna and P. Skands, JHEP **0605**, 026 (2006); version 6.409 was used.
[12] S. Höche *et al.*, *"Matching Parton Showers and Matrix Elements"*, in Proceedings of the Workshop on the Implications of HERA for LHC Physics, ed. A. De Roeck and H. Jung (CERN, Geneva, 2005), p288.
[13] V.M. Abazov *et al.* (D0 Collaboration), Phys. Rev. Lett. **100**, 102002 (2008).
[14] K. Melnikov and F. Petriello, Phys. Rev. D**74**, 114017 (2006).
[15] E. Boos *et al.* (CompHEP Collaboration), Nucl. Instrum. Methods in Phys. Res. A **534**, 250 (2004).
[16] J. Pumplin *et al.*, JHEP **0207**, 012 (2002); D. Stump *et al.*, JHEP **0310**, 046 (2003).
[17] J.M. Campbell and R.K. Ellis, Phys. Rev. D **60**, 113006 (1999).
[18] M. Cacciari *et al.*, JHEP **404**, 068 (2004); N. Kidonakis and R. Vogt, Phys. Rev. D **68**, 114014 (2003); N. Kidonakis, Phys. Rev. D **74**, 114012 (2006).
[19] T. Hahn *et al.*, *"SM and MSSM Higgs Boson Production Cross Sections at the Tevatron and the LHC"*, `arXiv:hep/ph:0607308`.
[20] R. Brun and F. Carminati, CERN Program Library Long Writeup W5013, 1993 (unpublished).
[21] D0 Collaboration, *"A search for associated production of a b quark and a neutral Higgs boson which decays to taus in supersymmetric models"* D0 Note 5985-CONF (2009).
[22] T. Scanlon, *"b-Tagging and the Search for Neutral Supersymmetric Higgs Bosons at D0"*, FERMILAB-THESIS-2006-43.
[23] L. Breiman *et al.*, *"Classification and Regression Trees"*, Wadsworth (1984); Y. Freund and R.E. Schapire, *"Experiments with a new boosting algorithm"*, in Machine Learning: Proceedings of the Thirteenth International Conference, pp. 148-156 (1996); V.M. Abazov *et al.*, Phys. Rev. Lett. **98**, 181802 (2007).
[24] T. Junk, Nucl. Instrum. Methods in Phys. Res. A **434**, 435 (1999); A. Read, in *"1st Workshop on Confidence Limits"*, CERN Report No. CERN-2000-005, 2000.
[25] W. Fisher, *"Systematics and limit calculations"*, FERMILAB-TM-2386-E (2006).